

Effects of aliasing on the fidelity of a two dimensional array of foci generated with a kinoform

D. R. Burnham, T. Schneider, and D. T. Chiu*

Department of Chemistry, University of Washington, Box 351700 Seattle, Washington
98195-170, USA

*chiu@chem.washington.edu

Abstract: This paper investigates, through simulation and experiment, the behavior of two dimensional foci arrays generated via phase-only holography where an iterative algorithm was used to produce the kinoforms. Specifically, we studied how aliasing of the signal on a spatial light modulator affects the quality of the foci array as the density and size of the array are varied. This study provides a reference for applications where it is important to understand how the fidelity and overall quality of the foci array changes as the number of foci increases and as the spacing between foci decreases.

© 2011 Optical Society of America

OCIS codes: (050.1970) Diffractive optics; (070.6120) Spatial light modulators; (090.1995) Digital holography.

References and links

1. D. Gabor, "Microscopy by reconstructed wave-fronts," *Proc. R. Soc. London Ser. A* **197**, 454–487 (1949).
2. G. D. Love, "Wave-front correction and production of Zernike modes with a liquid-crystal spatial light modulator," *Appl. Opt.* **36**, 1517–1524 (1997).
3. K. L. Tan, W. A. Crossland, and R. J. Mears, "Dynamic holography for optical interconnections. I. Noise floor of low-cross-talk holographic switches," *J. Opt. Soc. Am. A* **18**, 195–204 (2001).
4. L. B. Lesem, P. M. Hirsch, and J. A. Jordan, Jr, "The kinoform: a new wavefront reconstruction device," *IBM J. Res. and Dev.* **13**, 150–155 (1969).
5. W. Xu, M. H. Jericho, I. A. Meinertzhagen, and H. J. Kreuzer, "Digital in-line holography of microspheres," *Appl. Opt.* **41**, 5367–5375 (2002).
6. B. Chang, L. Chou, Y. Chang, and S. Chiang, "Isotropic image in structured illumination microscopy patterned with a spatial light modulator," *Opt. Express* **17**, 14710–14721 (2009).
7. G. Gibson, D. M. Carberry, G. Whyte, J. Leach, J. Courtial, J. C. Jackson, D. Robert, M. Miles, M. Padgett, "Holographic assembly workstation for optical manipulation," *J. Opt. A, Pure Appl. Opt.* **10**, 044009 (2008).
8. W. H. Lee, "Sampled Fourier transform hologram generated by computer," *Appl. Opt.* **9**, 639–643 (1970).
9. G. Whyte and J. Courtial, "Experimental demonstration of holographic three-dimensional light shaping using a Gerchberg-Saxton algorithm," *N. J. Phys.* **7**, 117 (2005).
10. G. Sinclair, P. Jordan, J. Courtial, M. Padgett, J. Cooper, and Z. J. Laczik, "Assembly of 3-dimensional structures using programmable holographic optical tweezers," *Opt. Express* **12**, 5475–5480 (2004).
11. J. E. Curtis, C. H. J. Schmitz, and J. P. Spatz, "Symmetry dependence of holograms for optical trapping," *Opt. Lett.* **30**, 2086–2088 (2005).
12. R. di Leonardo, F. Ianni, and G. Ruocco, "Computer generation of optimal holograms for optical trap arrays," *Opt. Express* **15**, 1913–1922 (2007).
13. J. W. Goodman, *Introduction to Fourier Optics*, 3rd Ed. (Roberts and Company Publishers, 2005).
14. C. H. J. Schmitz, J. P. Spatz, and J. E. Curtis, "High-precision steering of multiple holographic optical traps," *Opt. Express* **13**, 8678–8685 (2005).
15. Y. Takaki and J. Hojo, "Computer-generated holograms to produce high-density intensity patterns," *Appl. Opt.* **38**, 2189–2195 (1999).

16. C. Kohler, X. Schwab, and W. Osten, "Optimally tuned spatial light modulators for digital holography," *Appl. Opt.* **45**, 960–967 (2006).
 17. K. D. Wulff, D. G. Cole, R. L. Clark, R. Di Leonardo, J. Leach, J. Cooper, G. Gibson, and M. J. Padgett, "Aberration correction in holographic optical tweezers," *Opt. Express* **14**, 4169–4174 (2006).
 18. J. Amako, H. Miura, and T. Sonehara, "Speckle-noise reduction on kinoform reconstruction using phase-only spatial light modulator," *Appl. Opt.* **34**, 3165–3171 (1995).
-

1. Introduction

Holograms are used in many areas, including three-dimensional image formation [1], wavefront correction [2], and optical interconnects [3]. More recently phase-only holograms, or kinoforms [4], have attracted much interest for use in microscopy-based techniques, including digital holographic microscopy [5], structured illumination [6], and optical manipulation [7]. For many of these applications, static kinoforms [8] have given way to dynamic implementations using spatial light modulators (SLMs) [9]. These devices enable real-time modulation of kinoforms and thus allow time varying processes to be implemented [10], such as forming and changing the positions of multiple optical traps in real time.

For many of these applications, it is important to understand what limits the complexity of the patterns that can be formed using kinoforms. In the context of parallel optical trapping, a body of work has been carried out with the aim of optimizing the generation of an array of laser foci for manipulating micro- and nanoparticles [11, 12]. For optical trapping, the number of foci is often limited by the amount of laser power that the SLM can tolerate, because each laser focus must have sufficient power for trapping. For imaging applications, such as in spatial patterning of illumination, the laser powers involved are typically much lower than in optical trapping. As a result, the number of laser foci is no longer constrained by laser power, but by the accuracy of the kinoform used to generate a large number of foci that are closely spaced.

Kinoforms displayed on SLMs are effectively discretized versions of the ideal solution used to form the foci array. Therefore, it is important to understand the effects any aliasing may have upon the arrays produced. As with any spatially varying signal, it must sample the original signal at or above the Nyquist frequency to prevent aliasing. Finding the solution from an iterative algorithm gives no analytical description of the kinoform, so it is impossible to predict when aliasing will degrade the resulting image. As such we decided to undertake an empirical study to understand how aliasing affects the quality of the 2D foci array, specifically when the foci become very dense and also large in number.

Figure 1 depicts the setup we used for this study. Here, the system uses the standard configuration of a Fourier transform lens placed one focal length from the kinoform to produce foci in the back focal plane of the lens [13]. In our experiments, this image is de-magnified onto the focal plane of a microscope. The array parameters are described by the inter-foci spacing, d_x , the number of laser foci, N_{foci} , and the maximum spatial frequency, f_{max} .

In most applications, regardless of whether the intensity pattern is for optical trapping or fluorescence imaging, the desired foci array is known and the corresponding kinoform must be found, a classic inverse problem. Analytical solutions exist using superposition algorithms that allow foci to be placed < 10 nm apart [14], but this approach quickly produces poor kinoforms for foci number $\gtrsim 10$. For larger arrays, an iterative-type weighted Gerchberg-Saxton algorithm, with a superposition starting phase, provides the best result in terms of uniformity of the generated foci, efficiency, and relative standard deviation (rel. σ) of foci intensities [12]. However, this method limits the spacing between foci to $\delta_x = (\lambda f_1 f_{obj}) / (f_2 a \sqrt{N_{pix}})$, where f_1 is the focal length of the transform lens, f_2 is the focal length of the second lens, λ is the wavelength of light, a is the pixel pitch of the SLM, and N_{pix} is the number of pixels in the kinoform [15]. It is this iterative algorithm we concentrate on here.

De-coupling the inter-dependent parameters - density of foci, ρ_{foci} , number of foci, N_{foci} ,

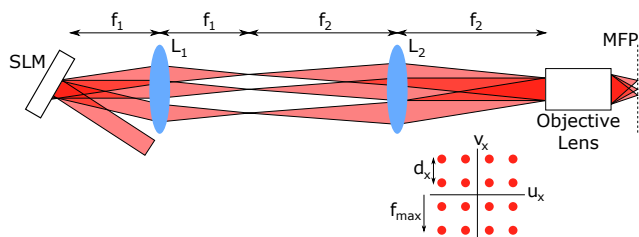


Fig. 1. The holography apparatus is constructed with a 4f system. L_1 is the Fourier transform lens, L_2 is a second lens, $f_1 = 300$ mm, $f_2 = 500$ mm. Inset shows our definitions of maximum spatial frequency, f_{max} , and inter-foci spacing, d_x , within the microscope focal plane (MFP).

maximum spatial frequency, f_{max} , and inter-foci spacing, d_x - is not possible, so we approached the problem by asking two main questions that are pertinent to our aims. First, for a given d_x , what effect does varying N_{foci} have? Second, for a given fixed f_{max} , what effect does increasing ρ_{foci} have?

For our study the non-aliased ‘original’ kinoform was created through the iterative algorithm because an exact solution does not exist. We also chose to study symmetric square patterns centered on the 0^h order. To determine the size of original kinoform that we needed in our studies, kinoforms were calculated with a fixed set of parameters and with increasing number of pixels in the result, N_{orig} , after which consecutive original kinoforms were compared through the mean residual of their differences. As an example, Fig. 2 shows increasing N_{orig} reduced the difference between consecutive kinoforms. For larger inter-foci spacing, convergence occurred for larger N_{orig} . From this set of calculations, we determined kinoforms calculated with $\sqrt{N_{orig}} = 2000$ should be sufficient to represent the true signal.

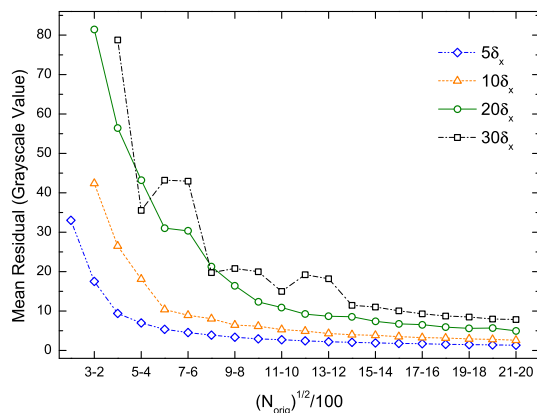


Fig. 2. Root mean square residual difference between original kinoforms with $\sqrt{N_{orig}} = 100P$ and $\sqrt{N_{orig}} = 100(P - 1)$ where P are integers between 1 and 21. Here $N_{foci} = 100$ and d_x is varied between $5\delta_x$ and $30\delta_x$.

Fourier transforming the kinoform with flat-top uniform incident light, normalized to an intensity of unity, simulates the optical system shown in Fig. 1, thereby allowing us to examine and compare the intensities of the foci with our experimental results. The quality of foci arrays produced are quantified using the rel. σ of foci intensities in the array, which has been shown to

be a reliable metric of pattern quality [12]. The aliased kinoform was constructed by sampling every $\sqrt{N_{orig}/N_{al-pix}}$ pixels while retaining the same size of the original kinoform (Fig. 3).

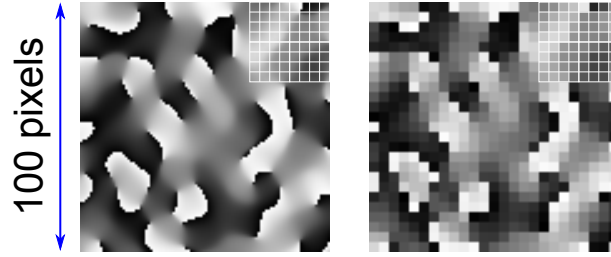


Fig. 3. Left panel: A 100×100 pixel section of original kinoform with $\sqrt{N_{orig}} = 2000$. Right panel: Same section of the original kinoform aliased to $\sqrt{N_{al-pix}} = 500$ pixels. One pixel in the right panel has the same physical dimension as 16 pixels in the left panel. Both white grids in the upper right corner of the panel display boxes that are 4×4 original pixels in size.

In Fig. 4, with $d_x = 10\delta_x$, the quality of the simulated foci array is plotted as a function of N_{foci} for several N_{al-pix} . It can be seen rel. σ increases with N_{foci} , and the inset shows, for $N_{foci} = 400$, aliasing the kinoform below 1000^2 pixels results in a rapid decrease in quality.

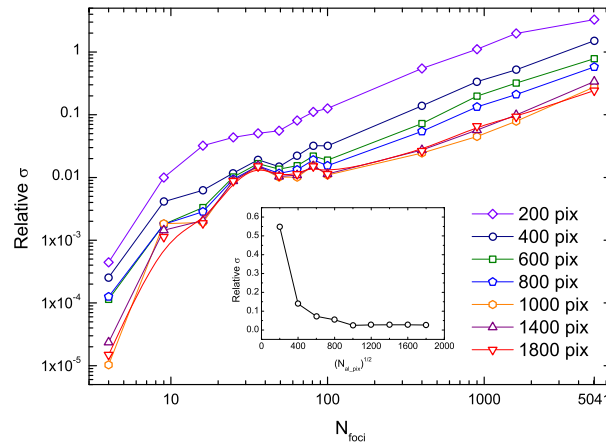


Fig. 4. Simulated relative standard deviation of foci intensities (rel. σ) versus increasing number of foci (N_{foci}) for kinoforms with varying numbers of aliased pixels (N_{al-pix}) and $d_x = 10\delta_x$. The legend indicates N_{al-pix} for each curve. Inset shows the effect of aliasing on rel. σ for $N_{foci} = 400$.

Figure 5 plots the quality of the foci array as a function of ρ_{foci} when the original kinoform was aliased to several N_{al-pix} and with $f_{max} = 30\delta_x$. After an initial increase in rel. σ , counter-intuitively, there exists a threshold in density above which the quality of the kinoform remained approximately equal. The inset shows, for $\rho_{foci} = 0.071$ foci μm^{-2} , when aliased below 1000^2 pixels there was a rapid decrease in the quality of the kinoform.

To test the findings experimentally we constructed an optical system as in Fig. 1. A c.w. 1064 nm laser (YLD-10-LP, IPG Photonics Corp.), power controlled using a $\lambda/2$ plate and polarizing beam cube, was expanded to fill the short axis of an SLM (Holoeye PLUTO NIR). A second $\lambda/2$ plate was used to optimize the diffraction efficiency through varying the polarization incident on the SLM. To image the foci array, we placed a mirror at the focal plane of the objective

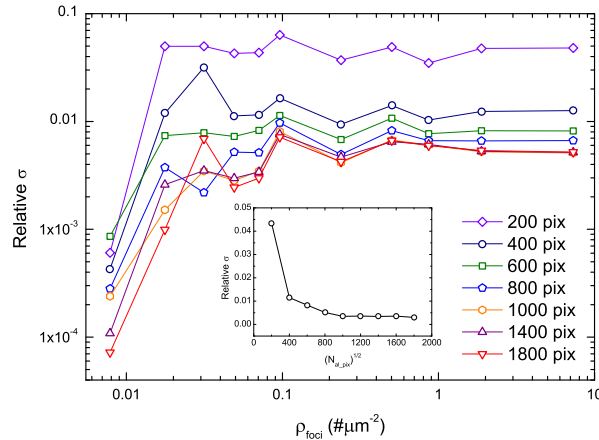


Fig. 5. Simulated relative standard deviation of foci intensities (rel. σ) plotted as a function of the density of foci (ρ_{foci}) for kinoforms with varying numbers of aliased pixels (N_{al-pix}) and for f_{max} (maximum spatial frequency) = $30\delta_x$. The legend indicates N_{al-pix} for each curve. Inset shows the effects of aliasing on pattern quality for a single $\rho_{foci} = 0.071 \text{ foci } \mu\text{m}^{-2}$.

to image the reflection of the formed foci. The SLM was imaged using a 4f system to slightly overfill the back aperture of a $40\times$ NA=1.4 Nikon Plan Fluor objective. Images were taken using a GC1380 GigE camera (Allied Vision Technologies) and analysis carried out with custom written LabVIEW software (v8.6 National Instruments Corp.), which measured the intensities of each foci and calculated their standard deviation relative to the mean intensity.

The SLM was calibrated to give a linear phase retardation response up to a maximum of 2π as a function of gray value applied [16]. Any non-flatness in the device was removed by using Zernike polynomials to create a correction kinoform [17] encoded into the test kinoforms, which produced a 2.200 ± 0.002 fold increase in Strehl ratio.

The original kinoforms used for Fig. 4 were first aliased to $\sqrt{N_{orig}} = 1080$ then test holograms were made for $N_{al-pix} = 200$ and 1080. These were displayed on the SLM and images taken of the resulting intensity patterns in the focal plane of the microscope. Figure 6 shows the measured rel. σ for several N_{foci} ; note only two differing N_{al-pix} are shown for clarity. Figure 6 indicates the same power-law trend is seen experimentally as in simulations. Experimentally we observed heavily aliased kinoforms performed comparably to the larger N_{al-pix} until $N_{foci} \approx 50$. The inset shows aliasing begins to severely affect pattern quality when $N_{al-pix} \lesssim 600^2$ pixels.

Finally kinoforms of Fig. 5 were aliased in a similar fashion and placed on the SLM to generate the experimental measurements shown in Fig. 7. Again, only two different N_{al-pix} are shown for clarity. Here, we observed rel. σ increased consistently with ρ_{foci} . Kinoforms with less aliasing performed better overall with performance again rapidly decreasing for $N_{al-pix} \lesssim 600^2$.

Experimentally the measurements indicate a poorer performance than that expected from simulation. We believe this is partly attributed to an increasing amount of speckle, known to occur in kinoform reconstruction [18], as the pattern complexity increases. Future studies should investigate the effectiveness of utilising a dummy area to improve precision [15].

Through simulations and experiments, we have characterized and given the first reference on how iteratively generated kinoforms perform at producing large or dense 2D arrays of laser foci. There are no limits on N_{foci} and d_x (above δ_x) per se, but as we have shown here, one must carefully balance the quality of the intensity pattern needed for the application with N_{foci}

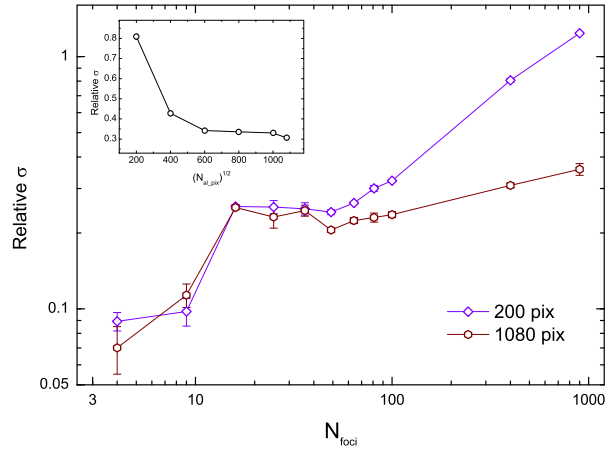


Fig. 6. Experimentally measured relative standard deviation of foci intensities (rel. σ) plotted as a function of the number of foci (N_{foci}) for N_{al-pix} (number of aliased pixels) = 200 and 1080; $d_x = 10\delta_x$. Inset shows the effect of aliasing on rel. σ for $N_{foci} = 400$. Error bars represent standard deviation; $n = 20$.

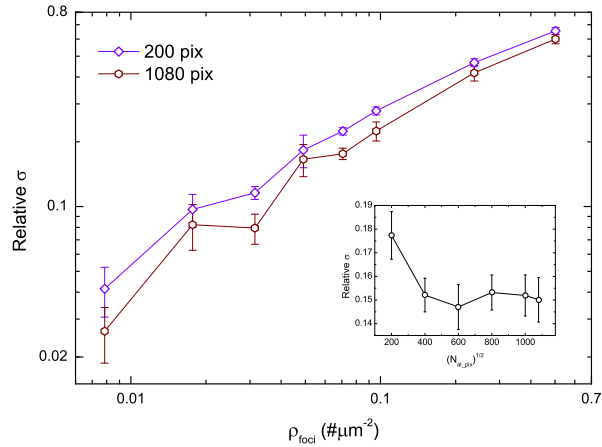


Fig. 7. Experimentally measured relative standard deviation of foci intensities (rel. σ) for varying foci density (ρ_{foci}); N_{al-pix} (number of aliased pixels) = 200 and 1080; f_{max} (maximum spatial frequency) = $30\delta_x$. Inset shows the effect of aliasing on rel. σ for $\rho_{foci} = 0.071$ foci μm^{-2} . Error bars represent standard deviation; $n = 20$.

and d_x . Finally, our studies show kinoforms need at least $\approx 600^2$ pixels to accurately represent the kinoform desired. This study should serve as a useful reference for applications, such as parallel confocal imaging or patterned illumination, in which it is important to understand how aliasing affects the degradation of the quality of the arrayed laser foci as the number or density of the foci is increased.

Acknowledgments

We thank Xudong Chen for many useful discussions. We are grateful to the NIH (GM 085485) for support of this work.